文章编号：1001-9014(2025)03-0352-06

DOI:10.11972/j.issn.1001-9014.2025.03.004

A near-infrared all-fiber mode monitor based on the mini-two-path Mach-Zehnder interferometer

ZHU Xiao-Jun[1], LIU Yu[1], WU Yue[1], ZHUANG Hao-Ran[1], SUN Dan[2], SHI Yue-Chun[3], CAO Juan[1*], YANG Yong-Jie[1*]

(1. School of Microelectronics and Integrated Circuits, Jiangsu Key Laboratory of Semi. Dev. & IC Design, Package and Test, Nantong University, Nantong 226019, China;
2. Peking University Yangtze Delta Institute of Optoelectronics, Nantong 226019, China;
3. Yongjiang Laboratory, Ningbo 315202, China)

Abstract: A novel near-infrared all-fiber mode monitor based on a mini-two-path Mach-Zehnder interferometer (MTP-MZI) is proposed. The MTP-MZI mode monitor is created by fusing a section of (no-core fiber, NCF) and a (single-mode fiber, SMF) together with an optical fiber fusion splicer, establishing two distinct centimeter-level optical transmission paths. Since the high-order modes in NCF transmit near-infrared light more sensitively to curvature-induced energy leakage than the fundamental mode in SMF, the near-infrared high-order mode light leaks out of NCF when the curvature changes, causing the MTP-MZI transmission spectrum to change. By analyzing the relationship between the curvature, transmission spectrum, and spatial frequency spectrum, the modes involved in the interference can be studied, thereby revealing the mode transmission characteristics of near-infrared light in optical fibers. In the verification experiments, higher-order modes were excited by inserting a novel hollow-core fiber (HCF) into the MTP-MZI. When the curvature of the MTP-MZI changes, the near-infrared light high-order mode introduced into the device leaks out, causing the transmission spectrum to return to its original state before bending and before the HCF was spliced. The experimental results demonstrate that the MTP-MZI mode monitor can monitor the fiber modes introduced from the external environment, providing both theoretical and experimental foundations for near-infrared all-fiber mode monitoring in optical information systems.

Key words: near-infrared mode monitor, Mach-Zehnder interferometer, two-path structure, all-fiber-format

基于微双臂马赫-曾德尔干涉仪的近红外全光纤模式监测器

朱晓军[1], 刘 宇[1], 吴 越[1], 庄浩然[1], 孙 丹[2], 施跃春[3], 曹 娟[1*], 杨永杰[1*]

(1. 南通大学 微电子学院(集成电路学院),半导体器件与集成电路设计封测省高校重点实验室,江苏 南通 226019;
2. 北京大学长三角光电科学研究院,江苏 南通 226019;
3. 甬江实验室,浙江 宁波 315202)

摘要:提出了一种基于微双臂马赫-曾德干涉仪(MTP-MZI)的新型近红外全光纤模式监测器。该MTP-MZI模式监测器通过光纤熔接机将无芯光纤(NCF)和单模光纤(SMF)熔接耦合,形成两条独立的厘米级光传输路径。NCF中近红外高阶模式相较于SMF中基模对曲率变化引起的能量泄漏更敏感,因此曲率变化时,NCF中近红外高阶模式光泄漏,导致MTP-MZI透射光谱发生变化。通过分析器件的曲率、透射光谱和空间频谱的关系,可以研究曲率变化过程中参与干涉的模式,以揭示光纤中近红外光的模式传输特性。验证实验中,通过在模式监测器前熔接空芯光纤(HCF)激发高阶模式,曲率变化时引入的高阶模式光泄漏,透射光谱恢复至无弯曲且未接入HCF的状态。实验结果表明,MTP-MZI模式监测器能够监测外部引入的光纤模式,为近红外全光纤模态监测在光纤通信系统中的应用提供理论与实验依据。

Received date: 2024-10-17, **revised date**: 2024-12-07 **收稿日期**:2024-10-17,**修回日期**:2024-12-07

Foundation items: Supported by the Central Government Guidance on Local Science and Technology Development Funds (2023ZY1023), and the Six Talent Peaks Project in Jiangsu Province (KTHY-052).

Biography: ZHU Xiao-Jun, male, Dingxi, Prof, PhD. Research area involves fiber optic sensors and fiber lasers. E-mail: zhuxj0122@ntu.edu.cn.

[*] **Corresponding authors**: E-mail: cj@ntu.edu.cn, yang.yj@ntu.edu.cn.

关 键 词:近红外模式监测器;马赫-曾德尔干涉仪;双臂结构;全光纤结构
中图分类号:TN214 **文献标识码**:A

Introduction

With the continuous development of fiber optic communication technology, the demand for communication capacity is endless[1]. The Mode-Division Multiplexing (MDM) system[2] in near-infrared wavelength, as an effective method to expand communication capacity[3], has received extensive research in areas such as orbital angular momentum[4], p1hotonic integration[5] and few-mode lasers[6]. Besides, MDM is preferred in near-infrared application areas such as laser processing[7], optical sensing[8], and optical imaging[9]. Adopting MDM systems can improve laser beam quality, enhance sensor sensitivity, and reduce the complexity of optical imaging devices. In the process of multimode transmission, it is particularly important to detect modes.

In order to monitor the types and distribution of transmitted modes, the modes of near-infrared wavelength to be monitored need to be separated first from the optical signal. Traditional methods for near-infrared mode monitoring include imaging and numerical analysis. Imaging methods mainly include spatially and spectrally resolved imaging (S^2)[10] and cross-correlated imaging (C^2). In 2008, Rydberg et al. proposed the S^2 method[11]to quantify the number and types of modes transmitted in large mode-field optical fibers. In 2014, Demas et al. determined the distribution and the weights of modes in the fiber based on the C^2 method at the wavelength of 1 046 nm [12]. In 2015, Liang Jin Huang et al. proposed a method for separating the modes of a fiber laser beam at the wavelength of 1 073 nm [13]. By measuring the near-field and far-field intensity distributions of the fiber output beam and using numerical analysis, various combinations of mode coefficients are calculated.

In recent years, with the rapid development of burgeoning subjects such as optical field modulation, the realization of mode-specific optical field output based on fiber laser within near-infrared wavelength has received extensive attention. Among them, near-infrared all-fiber mode converters have become a research hotspot because of their small size and ease of integration[14]. In 2018, Wang et al. proposed a near-infrared fiber laser with transverse mode switching output based on mode-selective photonic lanterns. The mode-selective photonic lantern was used to excite the LP_{01}, LP_{11a}, LP_{11b}, LP_{21a}, LP_{21b}, and LP_{02} modes, respectively, achieving the transverse mode-switched output of the fiber laser[15]. In 2019, Zhang et al. proposed a mode-selective coupler based on elliptical-core FMF, which realized a seven-mode multiplexer based on the mode selection coupler in the C-band [16]. For various near-infrared all-fiber mode converters, detecting the modes involved is necessary [17-18]. However, the traditional imaging methods are not compatible with optical devices and lack an all-fiber structure. Numerical analysis methods face the challenges of the complexity of optical systems. Additionally, the aforementioned techniques for modes converting devices were only suitable for cases involving a few number of high-order modes. Currently, there is no relevant research available for analysis of large number of higher-order modes within near-infrared wavelength, especially for monitoring of them. Lately, Zhuang et al. utilized SMFs to prepare the MZI structure with miniaturized two paths for curvature sensing measurement, offering an effective approach to achieving high sensitivity with two-path MZI sensors near the wavelength of 1 550 nm [8]. However, its single-sensing experiment limits the application of the structure.

In this paper, we present a novel near-infrared all-fiber mode monitor based on a Mini-Two-Path Mach-Zehnder Interferometer (MTP-MZI). By observing the distribution of the transmission and spatial frequency spectra of the MTP-MZI, we can analyze the characteristics of the modes involved in the interference and thus achieve the all-fiber modes monitoring. In addition, by introducing additional higher-order modes into the input light by HCF and then allowing their leakage through the bending, the feasibility of the mode monitoring using MTP-MZI is demonstrated. The MTP-MZI based near-infrared mode monitor offers a compact solution for all-fiber mode monitoring. Moreover, integrating advanced technologies like deep learning with MTP-MZI can enhance qualitative mode analysis, potentially transforming multimode laser communications, where dynamic mode monitoring is essential.

1 Mode monitor working principle

The principal structure of the near-infrared all-fiber mode monitor is shown in Fig. 1(a). The MTP-MZI consists of two couplers and two transmission paths. The incident light enters the Coupler 1 region through the SMF and divides into two parts. One part of the light transmits as a fundamental mode in the SMF, and the other transmits as the multimode in the NCF. Due to the different optical path distance, the various modes produce a transmission phase shift in the two interference paths. The light interference occurs when the two-path light signal reaches Coupler 2. Therefore, we can obtain the interfering mode characteristics by analyzing the transmission and spatial frequency spectra of the MTP-MZI. When curvature occurs in the MTP-MZI, as shown in Fig. 1 (b), the fundamental mode in the SMF remains unchanged due to minimal bending, while the higher-order modes in the NCF are more sensitive to the bending. The curvature-induced leakage will cause interference fringe change. After analyzing the transmission spectrum of the output light and its spatial frequency spectrum, we can monitor the mode characteristics in the transmission path.

We use the beam propagation method to numerically

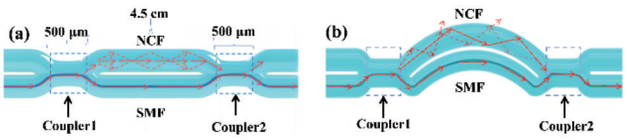

Fig. 1 Schematic diagram of the near-infrared all-fiber MTP-MZI mode monitor. :(a) flat MTP-MZI; (b) curved MTP-MZI
图1 近红外全光纤MTP-MZI模式监视器示意图:(a) 平直的MTP-MZI; (b)弯曲的MTP-MZI

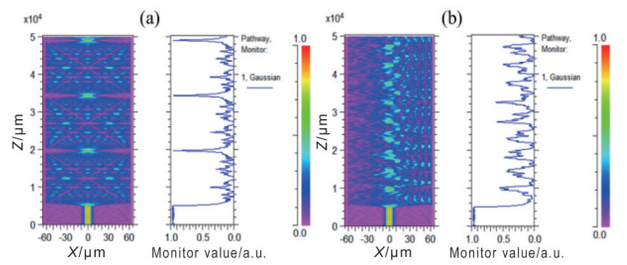

Fig. 2 Simulation of light field: (a) linear NCF; (b) curved NCF
图2 光场模拟仿真图:(a) 直线型NCF;(b) 弯曲型NCF

simulate the optical field distribution of the NCF. Figure 2 shows the optical field distribution of the NCF before and after bending. Comparatively, bending causes significant changes in NCF modes, with high-order mode leakage.

2 Fabrication and experimental results of the mode monitor

The proposed MTP-MZI can be fabricated only with a commercial fiber optic fusion splicer. The schematic diagram of the fabrication setup is shown in Fig. 3(a). The SMF features core and cladding diameters of 8.2 μm and 125 μm, respectively, and the NCF has a diameter of 125 μm. At first, the SMF and NCF are fixed side-by-side in the fixture of the fiber fusion splicer after stripping off their coating layer. To achieve a good coupling effect, it is necessary to pull the two optical fibers tightly and present both fibers on the same plane with the discharge electrode, as shown in Fig. 3(b). Then, the SMF and NCF are fused by the fiber fusion splicer in manual mode, whose discharge intensity is 250 bit and the discharge time is 2 500 ms. By conducting arc discharge on the two fibers, the coupling point of the two different optical fibers is shown in Fig. 3(c). We can see that the length of the coupling region is 500 μm, which is smaller than the conventional tapered coupling length of about 10 centimeters. Finally, by repeating the same operation, the MZI is obtained while the second coupling point is achieved. Since most of the operation of our structure is done automatically by the optical fiber splicer during the fabrication process, we can ensure that there is no gap between SMF and NCF during multiple experiments. And in the production process, we always maintain the same welding parameters, and the final coupling area is almost the same. Therefore, with the above process, we successfully fabricate the MZI with a mini-two-path of about 4.5 cm and two coupling regions of 500 μm. Compared with traditional linear MZI with a meter scale, our MTP-MZI is more compact and affordable. In addition, the MTA-MZI structure also has the advantage of the coupler-based two-path light splitting principle, providing constant optical energy distribution and precise and stable mode control.

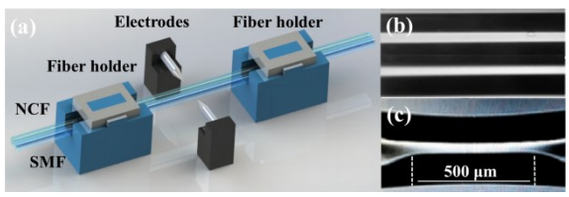

Fig. 3 (a) Schematic diagram of the preparation of the MTP-MZI coupling region; (b) the microscope image of NCF and SMF side-by-side positioned on the fusion splicer; (c) the microscope image of fusion region of NCF and SMF after discharge
图3 (a) MTP-MZI耦合区域的示意图;(b) NCF和SMF并排置于熔接机上的显微图;(c) 放电后NCF和SMF耦合区域显微图

Fig. 4 shows the experimental setup of the MTP-MZI for the fiber mode monitoring. We fixed the proposed mode monitor onto a flexible thin steel ruler and secured it to a precision translation stage using fixtures. The position of the displacement stage was slowly controlled by a micrometer screw to act precisely at the center of the steel ruler, inducing slight deformations in the ruler to achieve precise control over the curvature of the MTP-MZI. The input port of the MTP-MZI is linked to a Broadband light Source (BBS), while its output port is linked to an Optical Spectrum Analyzer (OSA) boasting a resolution of 0.02 nm. The curvature of the whole MTP-MZI can be calculated as:

$$C = \frac{1}{R} = \sqrt{\frac{2x}{x^2 + L^2}} \quad , \quad (1)$$

where x is the displacement of the precision displacement stage, L is the distance between fixtures, R is the radius of curvature and C is the curvature.

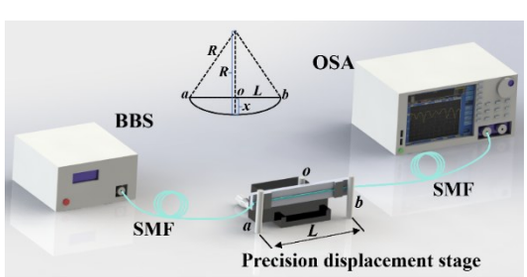

Fig. 4 The experiment setup of the MTP-MZI with curvature changing
图4 MTP-MZI曲率实验装置图

Figure 5 illustrates the experimental and validation flow of the MTP-MZI all-fiber mode monitor. Figure 5(a) shows the initial state of the MTP-MZI. In Fig. 5(b), the MZI is in a bent state. The high-order modes in

NCF leak due to bending, resulting in changes in the transmission spectrum and thus the phenomenon of mode hopping. To validate the MTP-MZI can monitor higher-order modes, the HCF is inserted in the input of MTP-MZI to excite higher-order modes, as shown in Fig. 5 (c). In Fig. 5(d), after bending, the modes in MTP-MZI returns to its original state. Experiment shows that higher-order modes can accurately be filtered, and the MTP-MZI can monitor input modes effectively.

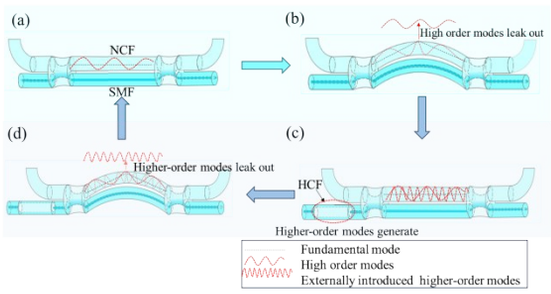

Fig. 5 Flow chart of MTP-MZI model monitoring experiment: (a) initial state of the mode monitor; (b) mode characterization experiments with MTP-MZI bending; (c) introduction of higher-order modes; (d) experimental validation of mode monitoring
图 5 MTP-MZI 模式监测实验流程图:(a) 模式监测器初始状态;(b) 模式监测器特性;(c) 引入高阶模式;(d) 实验验证模式监测

In the experiment of this paper, we choose the near-infrared band range from 1 525 nm to 1 610 nm. Fig. 6 presents transmission and spatial frequency spectra of the mode monitor with curvature increasing from 0 m^{-1} to 0.078 37 m^{-1}. In Fig. 6(a), the intensity of each wavelength dip changes as the curvature gradually increases. For example, the intensity of Dip 1 changes from -35 dB to -30 dB, but the wavelength position and the number of the dips of the whole spectra do not change. In Fig. 6 (b), many peaks exist in the spatial frequency, where the highest peak (0 Hz) corresponds to the fundamental mode of LP_{01}, the second highest peaks (smaller frequency) correspond to the dominant transmission modes and the remaining peaks correspond to the weak transmission modes. The spatial frequency spectra of the MTP-MZI show one primary high-order mode and two secondary high-order modes. As the curvature increases, the peaks corresponding to the primary higher-order modes decrease, which indicates that the higher-order modes are leaking. By comparing the transmission and spatial frequency spectra of the MTP-MZI in Fig. 6, it is clear that the MTP-MZI is highly sensitive to curvature. Even a slight change in curvature can be detected through the intensity change of each mode. Therefore, it can be employed as a mode monitor in multimode systems.

Figure 7 shows the transmission and corresponding spatial frequency spectra of the different curvatures of the MTP-MZI. In Fig. 7(a), the mode hopping phenomenon occurs as the curvature changes from 0.626 47 m^{-1} to 1.042 72 m^{-1}, with the Dip2 transitioning into a peak (the green dashed rectangle). This means that the

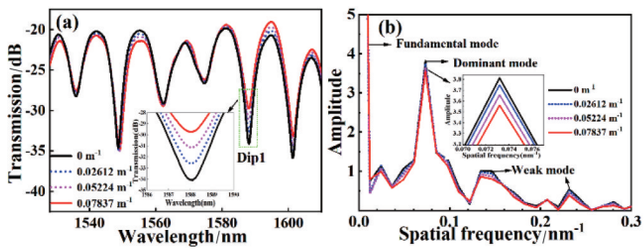

Fig. 6 (a) The transmission spectra of MTP-MZI with variation curvatures; (b) the corresponding spatial frequency spectrum
图 6 (a) 不同曲率 MTP-MZI 的透射光谱;(b) 相应的空间频谱

modes in MTP-MZI have changed, as shown in Fig. 7 (b), the energy of the dominant higher-order modes is gradually coupled into the lower-order modes as the curvature increases. As curvature changes from 1.842 56 m^{-1} to 2.326 41 m^{-1}, the mode hopping phenomena also occurs in Fig. 7(c). In Fig. 7(d), most minor modes are leaked. Experiments show that the functions of mode conversion and higher-order mode filtering is realized by bending the MTP-MZI structure.

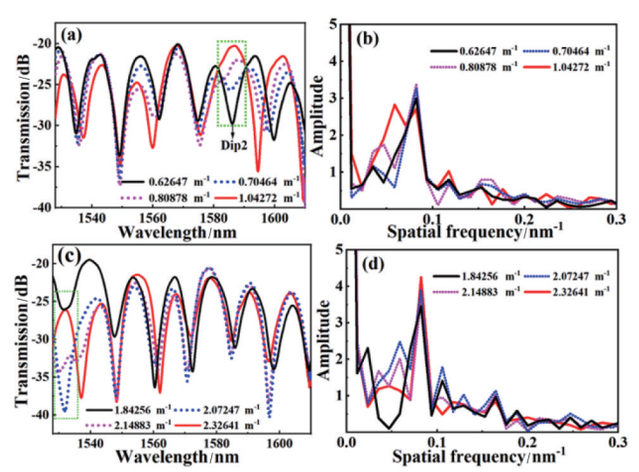

Fig. 7 (a) Transmission spectra with curvature range from 0.626 47 m^{-1} to 1.042 72 m^{-1}; (b) the corresponding spatial frequency spectra; (c) transmission spectra with curvature range from 1.842 56 m^{-1} to 2.326 41 m^{-1}; (d) the corresponding spatial frequency spectra
图 7 (a)曲率在 0.626 47 ~1.042 72 m^{-1} 范围的透射光谱;(b)相应的空间频谱;(c)曲率在 1.842 56 ~2.326 41 m^{-1} 范围的透射光谱;(d)相应的空间频谱

On this basis, we expect to test whether newly added higher-order modes can be leaked by bending the MTP-MZI structure. If the transmission spectrum is reduced to the initial transmission spectrum where the input is fundamental mode light, then it can be determined that the externally introduced higher-order modes are entirely encompassed within the leaked higher-order modes. By the qualitative analysis of the modes, monitoring of the input light modes can be achieved. So, we carried out validation experiments.

A section of HCF is fused in front of the MTP-MZI

structures to excite high-order modes. Other types of fibers can be used in place of HCF, but new interference cannot be generated during the mode excitation process, otherwise the newly generated interference spectrum will overlap with the transmission spectrum of the MTP-MZI. In Fig. 8(a), we compare the transmission spectra before and after adding HCF in MTP-MZI. The black waveform is the initial transmission spectrum, which is represented by INIT, and the red waveform is the transmission spectrum for MTP-MZI with HCF. We can see that the increase in higher-order modes in the input light causes the dense wavelets to be superimposed on the original interference spectrum. Figure 8(b) shows the corresponding spatial frequency spectrum comparison. Compared to the initial spatial frequency spectrum, the spatial frequency spectrum changes from one dominant higher-order mode to two dominant modes after adding higher-order modes by HCF.

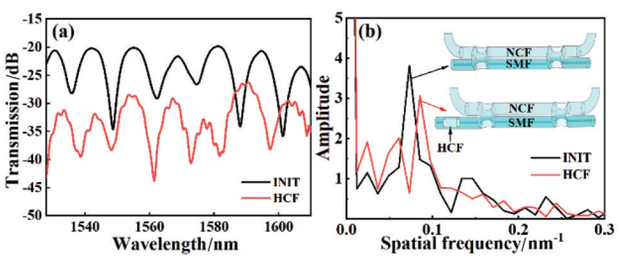

Fig. 8 (a) A comparison of the transmission spectra of the MTP-MZI without and with HCF; (b) the corresponding spatial frequency spectra
图8 (a)初始透射光谱和熔接HCF的MTP-MZI透射光谱;(b)相应的空间频谱

In Fig. 9(a) and (b), as curvature changes from 0.574 33 m^{-1} to 1.868 17m^{-1}, higher-order modes leakage occurs, and the wavelets in the transmission spectra gradually decrease even basically disappear. In Fig. 9(c), when the curvature is 2.225 04 m^{-1}, the transmission spectrum of MTP-MZI with HCF is basically the same as the initial spectrum without HCF. In Fig. 9(d), the curve distributions of the two structures are basically the same, and the spatial spectra are only slightly shifted in terms of the wavelengths, which indicates that the modes involved in the interference are the same in the two structures. It is worth noting that the difference between the initial black waveform and the red waveform in Fig. 9(c) and (d) is unavoidable. Due to the introduction of high-order modes by splicing HCF, there is an inevitable core diameter and mode mismatch between HCF and SMF, leading to transmission loss. After bending, the effective length of the interference path is increased, resulting in a smaller FSR.

By comparing Fig. 8 with Fig. 9, we illustrate the mechanism of the MTP-MZI in the mode monitor. Fusing an HCF in front of MTP-MZI, dense wavelets is superimposed on the original transmission spectrum, and new high-order modes appear in spatial frequency spectrum. When the curvature changes slightly, the transmission spectrum only shows intensity changes or slight wave-

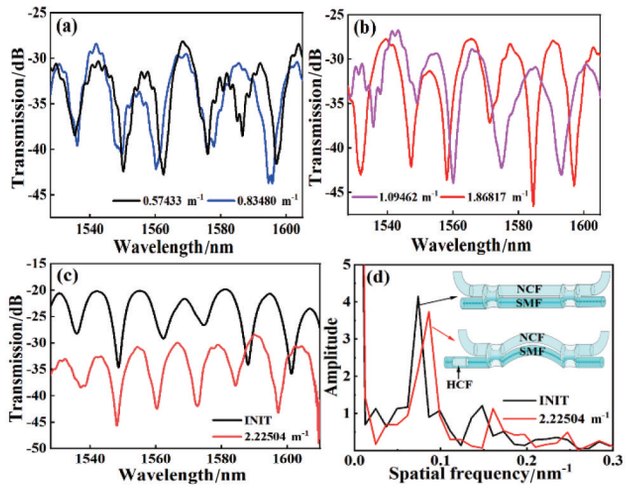

Fig. 9 (a) Transmission spectrum of the MTP-MZI with HCF at curvature of 0.574 33 m^{-1}, 0.834 8 m^{-1} and (b) 1.094 62 m^{-1}, 1.868 17 m^{-1}, respectively; (c) the transmission spectrum of the MTP-MZI with HCF at curvature of 2.225 04 m^{-1} and the straight MTP-MZI without HCF; (d) the corresponding spatial spectra
图9 (a)(b)曲率为0.574 33 m^{-1}和0.834 8 m^{-1}以及1.094 62 m^{-1}和1.868 17 m^{-1}的透射光谱;(c)带有HCF的曲率为2.225 04 m^{-1}的MTP-MZI透射光谱和初始透射光谱;(d)相应的空间频谱

length shifts. As the curvature increases, the mode hopping happens. Higher-order modes in the corresponding spatial frequency spectrum couple with lower-order modes. When the MTP-MZI is bent to a certain extent, the higher-order mode leakage occurs, and the dense wavelets on the transmission spectrum gradually disappear. The transmission and spatial frequency spectra essentially revert to the initial spectra before the fusion of the HCF. Therefore, the modes introduced externally are included in the modes corresponding to the curvature from the coupling of the higher-order subpeaks to the disappearance of the higher-order subpeaks. In the other words, the higher-order modes filtered out in this process are the newly added modes introduced externally by HCF. If we can statistically analyze all the modes of the MTP-MZI, we can quantitatively analyze the main modes involved in the interferometer from the transmission and spatial frequency spectra of the proposed structure, and monitor the unknown modes that mixed into the input signal.

At last, we conducted repeatability experiments to measure the reproducibility and stability of the structure. In the manuscript, we obtained two additional mode monitors using the same manufacturing process. The obtained transmission spectrum and corresponding spatial frequency are shown in Fig. 10(a) and (b), respectively. We can see that the transmission and corresponding spatial frequency spectrum show a high degree of similarity, indicating that the design is robust enough to handle such changes. Figure 10(c), (d), (e), and (f) show that after the same curvature adjustment, the MTP-MZI of Repeat 1 and 2 experiments can be approximately restored to the original spectrum after undergoing the same curvature adjustment and being connected to HCF, which indicates that these ex-

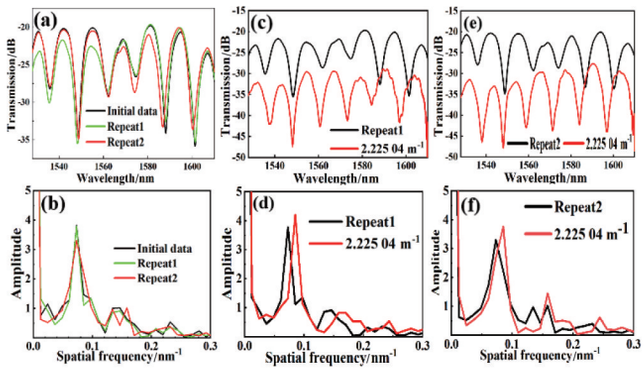

Fig. 10 (a) Initial transmission spectra of the original mode monitor, Repeat1, and Repeat2, respectively; (b) the corresponding spatial frequency spectra; (c) and (e) MTP-MZI transmission spectrum and initial transmission spectrum with HCF with curvature of 2.225 04 m^{-1} in Repeatability Experiments 1 and 2; (d) and (f) are the corresponding spatial spectra

图 10 (a) 初始透射谱, 重复性实验 1 和实验 2 的透射谱; (b) 相应的空间频谱; (c) 和 (e) 重复性实验 1 和 2 中带有 HCF 的曲率为 2.225 04 m^{-1} 的 MTP-MZI 透射光谱和初始透射光谱; (d)和 (f) 为相应的空间频谱

periments exhibit the expected monitoring performance, showcasing excellent robustness and repeatability of our structure.

3 Conclusion

In this paper, we proposed a centimeter-scale near-infrared all-fiber mode monitor based on MTP-MZI. By changing the curvature of the MTP-MZI, the curvature-induced leakage of the high-order mode in the NCF changed, causing variations in the transmission spectrum and corresponding spatial frequency spectrum. In the validation experiments, the higher-order modes are introduced by fusion splicing the HCF, and the higher-order modes are leaked after bending the MTP-MZI structure. The transmission and spatial frequency spectra were finally recovered to the spectra without connecting the HCF, which realized the monitoring of externally introduced modes. The proposed near-infrared mode monitor offers a new approach to the feasibility investigation of mode monitors with an all-fiber format. It also has several advantages, such as small size, high robustness, easy preparation, and low cost, making it ideal for various near-infrared wavelength field applications such as optical communication, laser processing, optical sensing, and imaging.

References

[1] KHONINA S N, KAZANSKIY N L, BUTT M A, et al. Optical multiplexing techniques and their marriage for on-chip and optical fiber communication: review [J]. Opto-Electronic Advances, 2022, 5(8): 210127-1-210127-25.
[2] JI Ke, CHEN He-Ming. Coarse wavelength-mode-division hybrid multiplexer/de-multiplexer of photonic crystal[J]. Journal of Infrared and Millimeter Waves, 2018, 37(1): 50-59.
季珂,陈鹤鸣.光子晶体粗波分-模分混合复用/解复用器[J].红外与毫米波学报, 2018, 37(1): 50-59.
[3] SOMA D, BEPPU S, WAKAYAMA Y, et al. 257-Tbit/s weakly coupled 10-mode C+ L-band WDM transmission [J]. Journal of Lightwave Technology, 2018, 36(6): 1375-1381.
[4] LIU Y, RISHØJ L S, GALILI M, et al. Orbital angular momentum data transmission using a silicon photonic mode multiplexer [J]. Journal of Lightwave Technology, 2023, 41(7): 2123-2130.
[5] XU H, DAI D, SHI Y. Silicon integrated nanophotonic devices for on-chip multi-mode interconnects [J]. Applied Sciences, 2020, 10(18): 6365.
[6] XIANG S, HAN Y, GAO S, et al. Semiconductor lasers for photonic neuromorphic computing and photonic spiking neural networks: A perspective [J]. APL Photonics, 2024, 9(7).
[7] DREVINSKAS R, ZHANG J, BERESNA M, et al. Laser material processing with tightly focused cylindrical vector beams [J]. Applied Physics Letters, 2016, 108(22).
[8] ZHU X, ZHUANG H, LIU Y, et al. High-sensitivity robust Mach-Zehnder interferometer sensor in ultra-compact format [J]. Measurement, 2024: 115051.
[9] BAUTISTA G, KAKKO J P, DHAKA V, et al. Nonlinear microscopy using cylindrical vector beams: Applications to three-dimensional imaging of nanostructures [J]. Optics Express, 2017, 25(11): 12463-12468.
[10] NICHOLSON J W, YABLON A D, FINI J M, et al. Measuring the modal content of large-mode-area fibers [J]. IEEE journal of selected topics in quantum electronics, 2009, 15(1): 61-70.
[11] RYDBERG C, BENGTSSON J. Numerical algorithm for the retrieval of spatial coherence properties of partially coherent beams from transverse intensity measurements [J]. Optics express, 2007, 15(21): 13613-13623.
[12] DEMAS J, RAMACHANDRAN S. Sub-second mode measurement of fibers using C 2 imaging [J]. Optics express, 2014, 22(19): 23043-23056.
[13] HUANG L, LENG J, ZHOU P, et al. Adaptive mode control of a few-mode fiber by real-time mode decomposition [J]. Optics express, 2015, 23(21): 28082-28090.
[14] YANG A, ZHU J, LIU X, et al. Integrated all-fiber structures for generating doughnut beam arrays and hollow Bessel-like beams [J]. Optics and Lasers in Engineering, 2022, 153: 107006.
[15] WANG N, ZACARIAS J C A, ANTONIO-LOPEZ J E, et al. Transverse mode-switchable fiber laser based on a photonic lantern [J]. Optics Express, 2018, 26(25): 32777-32787.
[16] ZHANG H, WANG Z, XI L, et al. All-fiber broadband multiplexer based on an elliptical ring core fiber structure mode selective coupler [J]. Optics Letters, 2019, 44(12): 2994-2997.
[17] FU C, LIAO Y, HE Y, et al. Design of TE_{01}-HE_{11} mode converter with TE_{11} as intermediary mode [J]. Journal of Infrared and Millimeter Waves, 2017, 36(1): 24-29.
[18] DING Y, LI J, LI S, et al. Eight modes selective elliptic-core photonic lantern in mimo-free mode division multiplexing systems at S+ C+ L bands [J]. Journal of Lightwave Technology, 2022, 41(2): 739-744.